Available online at www.sciencedirect.com
ScienceDirect
Mathematics and Computers in Simulation 209 (2023) 282–298
MATHEMATICS AND COMPUTERS IN SIMULATION
www.elsevier.com/locate/matcom

Original articles

Mathematical modeling and simulation of the inverse kinematic of a redundant robotic manipulator using azimuthal angles and spherical polar piecewise interpolation

Mihai Dupac

Department of Design and Engineering, Bournemouth University, Talbot Campus, Poole, BH12 5BB, UK

Received 2 November 2022; received in revised form 1 February 2023; accepted 14 February 2023
Available online 1 March 2023

Abstract

In this study, smooth trajectory generation and the mathematical modeling of the inverse kinematics and dynamics of a redundant robotic manipulator is considered. The path of the end-effector of the robotic manipulator is generated – along a particular set of via-points – in a system of spherical coordinates by combining the Hermite polar piecewise interpolants that approximate each intermediate radial distance on the reference plane using the azimuthal angle and each corresponding point height of the path computed in the rotating radial plane through the corresponding polar angle. The smoothness of the end-effector path is guaranteed by the use of quintic Hermite piecewise interpolants having functional continuity, while the inverse kinematics and inverse dynamics used to compute the coordinates of the joints and the equations of motion of the robotic manipulator are considered for optimum trajectory planning. Optimization solutions to minimize the joint velocities, the end-effector positioning error, the traveling time and mechanical energy, or the consumed power, are presented. The direct computation of the joints trajectory and a optimal trajectory with minimization of the end-effector position error while preserving trajectory smoothness of the joints are considered. To assess and verify the approach numerical examples – implemented in Matlab – are introduced, and the outcomes are examined.

Keywords: Mathematical modeling; Polar piecewise interpolation; Trajectory planning

1. Introduction

1.1. Background

Optimal trajectory planning, involving the generation of a smooth geometric path [12] along certain requirements and constraints play a crucial role in engineering design and robotics. The ability to generate a smooth motion along a sequence of target points under some kinematic and dynamic constraints (input) can be addressed through trajectory planning in the joint space, i.e., joint position, velocity, and acceleration (output) by inverse kinematics of the geometric path. Considering joint trajectories optimization techniques – such as minimum execution time, minimum jerk, or minimum energy [12], under by the assumed kinematic and dynamic constraints – is imperative especially when induced vibrations, execution time, and wear should be diminished.

E-mail address: mdupac@bournemouth.ac.uk.

https://doi.org/10.1016/j.matcom.2023.02.010

Nomenclature

r_{P_m}	The radial distance from the origin O to the projection of the point P_m on the plane Oxy
z_{P_m}	The height from the via-point P_m to the azimuthal plane Oxy
θ_{P_m}	The azimuthal angle
$\mathbf{i}$, $\mathbf{j}$, $\mathbf{k}$	The unit vectors of the Cartesian reference frame $Oxyz$
$\mathbf{i}_r, \mathbf{j}_r, \mathbf{k}_r$	The unit vectors of the moving reference frame $Ox_r y_r z_r$
d_i	The length of the rod (link) i
Φ_i	The joint (relative) angles of the robotic manipulator (between the links i and $i+1$)
$\dot{\Phi}_{\mathbf{i}}$	The angular velocity of the joints of the robotic manipulator
Φ	The absolute angle showing the end-effector direction
$\mathbf{J}(\Phi)$	The Jacobian matrix of the robotic manipulator
$z(\varphi)$	The height of the trajectory of motion computed in the rotating azimuthal plane
$r(\theta)$	The polar coordinates used to approximate the projected planar polar trajectory
$r(\theta)$, θ and $z(\varphi)$	The cylindrical coordinates used to parameterize the geometric path of the end effector
u_k^i	The Hermite polynomial coefficients used to compute the projected planar path of motion
s_k^i	The Hermite polynomial coefficients used to compute the height of the end-effector trajectory of motion
$\mathbf{r}$, $\mathbf{v}$ and $\mathbf{a}$	The position, velocity and acceleration vectors related to the geometric path of the end effector
$T(\Phi, \dot{\Phi})$	The kinetic energy of the manipulator.
$U(\Phi)$	The potential energy of the manipulator
$\mathcal{L}(\Phi, \dot{\Phi})$	The Lagrangian of the system
$\mathbf{r}_{0c_i}$	The position vector of the centroid of link i
$\mathbf{v}_{c_i}$	The velocity vector of the centroid of link i
ω_i	The angular velocity vector of the centroid of link i
$\mathbf{J}_i^L$	The centroidal linear velocity Jacobian matrix
$\mathbf{J}_i^A$	The centroidal angular velocity Jacobian matrix
$\mathbf{I}_i$	The inertia matrix of the ith link
$\mathbf{H}$	The multibody inertia matrix
τ_i	Joint torques of the manipulator links
M	The matrix of inertia of the matrix equation
$\hat{C}$ and $\tilde{C}$	The centripetal and the Coriolis force matrices
G_i	The gravity vector
$\mathcal{R}$	The objective function related either to the DLS, to the end-effector position error minimization, or to the minimum consumed power method
$\|.\|$	The associated euclidian norm of the DLS method
λ	The damping factor of the DLS method
w_i	The weighting factors used on the end-effector position error minimization method
$r_g(\theta)$ and $z_g(\phi)$	The generated end effector positions in the rotating azimuthal plane
$\mathcal{D}_j$	The variable used to minimize joint displacement along the trajectory
$\mathcal{V}_e$	The velocity of the end effector
$\mathcal{V}_j$	The angular joint displacement
τ_i	The torque of the ith joint
t_i	The time intervals corresponding to the motion between the via-points of the trajectory

1.2. Formulation of the problem

The main reason for the generation of this paper was the conceptualization of a new approach by which an optimal trajectory planning for of redundant robotic manipulators, their forward and inverse kinematic and dynamic can be formulated and solved. In general, the robotic manipulators used in industrial applications are dynamical systems which could experience significant displacements and rotations, therefore their control could be challenging. Highly accurate and robust control of redundant robotic manipulators without knowing kinematic models of robots have been addressed in [30] by zeroing neural networks activated by nonlinear functions. A functional control scheme was considered in [31] to address the motion control problem of a mobile robot using screw theory. To decrease the interaction force acting on the robot arm a constant speed control [31] determined by an inverse kinematics approach was explored. A recurrent neural network control framework of a redundant manipulator for concurrent obstacle avoidance and tracking control along a predefined reference path was presented in [16]. The forward and inverse dynamics and control of a underactuated mechanical system subjected to a set of holonomic and/or nonholonomic algebraic constraint equations – showing that the designed state trajectories could be effectively imposed by the use the inverse dynamic method – was considered in [23].

In addition, while the classical methods of kinematic or dynamic motion planning can be effectively used for the trajectories modeling of multibody mechanical systems, the use of new, different, and more adequate analytical techniques are needed. Since the motion along some desired via points can be described as a combination of rotations about a fixed point, the manipulator dynamics can be related to its geometry using the time dependent generalized coordinates expressed as spherical or cylindrical coordinates. Such a mathematical modeling of a robotic manipulator using a zenithal gnomic trajectory located on a projective plane and the related azimuthal trajectory generated by polar piecewise interpolation on the azimuthal plane was addressed in [7]. Possible trajectories generated by mix-matching polar piecewise interpolation (used to devise the radial trajectory) and Cartesian piecewise polynomials (used to calculate the related height in a normal plane unfolded along the radial trajectory of the motion) has been presented in [9]. However, the use of a new and better and more effective computational approach that approximate the trajectory radial distance using the azimuthal angles and the corresponding height through the corresponding polar angles computed in the rotating azimuthal plane is deemed necessary.

1.3. Literature survey

An optimal inverse kinematic solution for mechanical manipulators calculated based on the end-effector initial and final position and relative angular orientation error was considered in [32]. Optimal path planning which minimizes the end-effector position error of planar manipulators at every intermediate point along the path (Genetic Algorithm) and track the prescribed trajectory accurately (Pattern Search) is presented in [2]. A trajectory planning hybrid algorithm approach and Euclidean distance based on inverse kinematic solution and displacement error of a manipulator is proposed in [5] to resolve motion rate control for a smooth motion of the end effector.

Efficient trajectories planning for cyclic point to point tasks have been considered in [11], and while the kinematics, path planning and curve generation – essential for design and manufacturing efficiency – have been proposed in [10] the problem of inverse kinematics is yet to be considered. Inverse kinematic solutions for the most frequently seen industrial robots by direct manipulation of trigonometric equations have been discussed in [3].

A forward and inverse kinematic analysis has been proposed in [22] to compare the accuracy and repeatability of the obtained solutions. A trajectory planning and inverse kinematics solution based on deterministic global optimization method of the piecewise motion of joint variables [24] or on a homogeneous matrix transformation [25] was considered to determine [24] and respectively follow [34] the desired trajectory.

A trajectory planning and associated inverse kinematics having the acceleration form of the end-effector outlined as polynomials of high degree have been addressed in [4]. Smooth point-to-point trajectory planned in the joint space using high-order polynomial curves is considered in [33]. A general algorithm for parametric curves generation using interpolation techniques have been considered in [17], classical piecewise interpolation and alternative methods for conserving shapes and extensions of spline interpolation is discussed in [15], C^2 smoothness is evaluated in [25,29], and spherical interpolation and approximation is studied in [28]. A computational approach for shape-preserving of irregular data using cubic L_p spline interpolation is considered in [18]. Shape preserving characteristics of splines [19] due to the large effect of L_1 and L_2 norm and curvature are considerable important especially when polar

coordinates are used. A bicubic-spline interpolation representation on a spherical domain using a no-uniform grid was presented in [14]. The dynamics of a multi-axis robot considered in [1] is addressed through the development of the Lagrange–Euler equations of motion and by finding the optimal torque at each joint using analytical optimization analysis for a given set of parameters.

1.4. Scope and contribution of this paper

In this paper, the smooth trajectory generation along a prescribed number of via-points, inverse kinematics, and optimal trajectory planning for a redundant robotic manipulator is considered. The approached developed in this study is based on the combinations of adequate geometric considerations – such as manipulators geometry and related coordinate systems – and the use of spherical polar piecewise cubic interpolants in the modeling of the forward and inverse kinematic and dynamics.

While previous approaches to the kinematics and dynamics of robotic manipulators allows to modeling by mix-matching either

- a zenithal gnomic trajectory located on a projective plane and the related azimuthal trajectory generated by polar piecewise interpolation on the azimuthal angles [7]

- radial trajectory generated by polar piecewise interpolation and the related height in a normal plane unfolded along the radial trajectory of the motion [9]

the newly method presented in this paper generates a more efficient computational approach to mix-match the radial distance (using the azimuthal angles) and the corresponding height (using the corresponding polar angles computed in the rotating azimuthal plane), that is, only the azimuthal and corresponding polar angles are considered.

Thus, the trajectory of the end effector along a prescribed number of via-points is generated in a system of spherical coordinates by merging the Hermite-type polar interpolation functions computed in the rotating azimuthal and radial projective planes. The smoothness of the path is acquired by the use of quintic Hermite piecewise interpolation holding continuous derivatives. Optimization solutions to minimize the joint velocities, the end-effector positioning error, the traveling time and mechanical energy, or the consumed power, are surveyed.

The effectiveness of the method developed in this study is demonstrated by means of numerical simulations applied to the computation of the joints trajectory (and the optimal trajectory) of the manipulator end effector with end-effector position error minimization. To demonstrate the approach numerical computations and Matlab simulations have been performed and the results verified.

1.5. Organization of the paper

The mathematical modeling of the redundant robotic manipulator including the trajectory generations, the parametric model, the forward kinematic equations, the inverse kinematics put forward in a rotating azimuthal plane, and the inverse dynamics, is presented in Section 2. Section 3 considers some possible optimization techniques such as the damped least square (DLS) approach, the end-effector position error minimization, or the minimum consumed power. The results presented in Section 4 discuss the model-based performance of the redundant robotic manipulator and the calculated optimized trajectories, followed in Section 5 by the conclusion.

2. Mathematical modeling

2.1. Trajectory generation

The three dimensional position vector connecting the origin of the Cartesian reference frame $Oxyz$ and the via-points $P_m, m = 1, \ldots, n$ of the trajectory of the end effector is expressed by

$$\mathbf{r}_{P_m} = r_{P_m} \cos\theta_{P_m} \mathbf{i} + r_{P_m} \sin\theta_{P_m} \mathbf{j} + z_{P_m} \mathbf{k} \tag{1}$$

where $r_{P_m} = d\,(O, P_m)$ is the radial distance from the origin O to the projection of the point P_m on the radial plane Oxy, z_{P_m} is the height from the via-point P_m to the radial plane Oxy, and θ_{P_m} is the azimuthal angle specified in an anticlockwise direction.

To interpolate between the data specified by the via-points (Fig. 1.a), one can consider the combination between a polar piecewise interpolation which approximates the projected planar polar trajectory ($r\,(\theta)$) on the plane Oxy

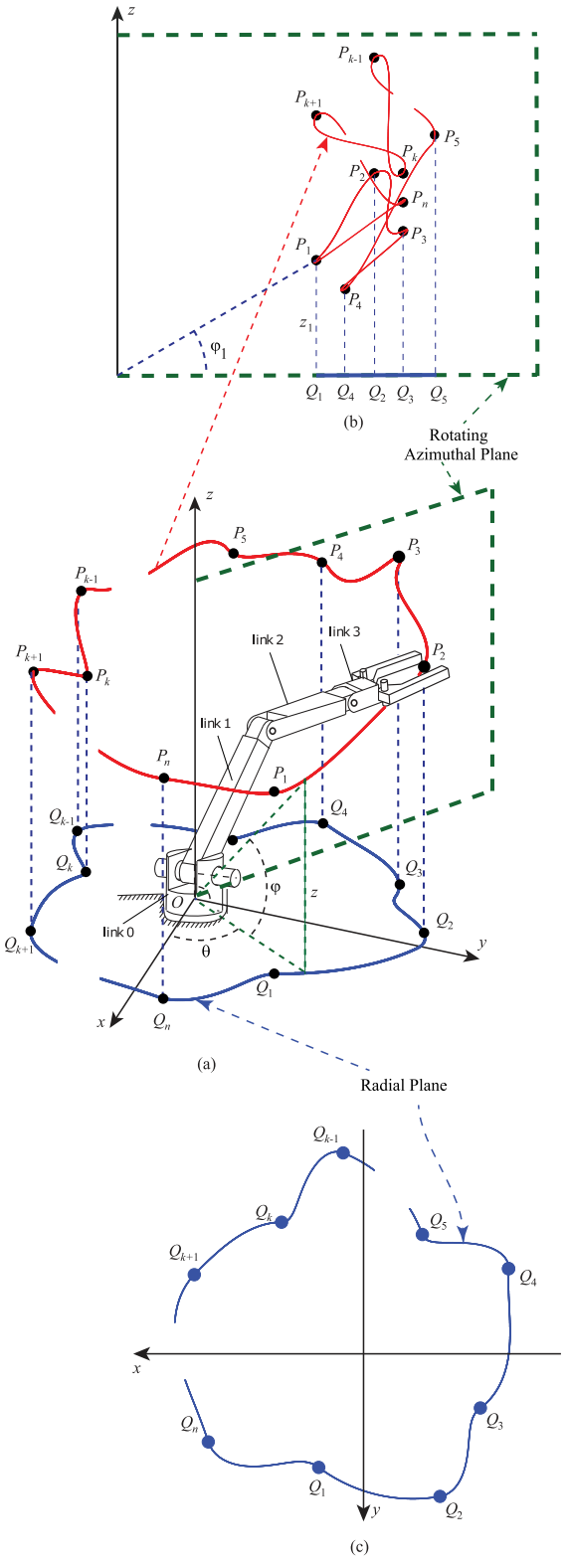

Fig. 1. Trajectory of the end effector expressed as a combination of piecewise polar Hermite-type function.

(Fig. 1.c) and a polar piecewise interpolation which approximate the height of the trajectory ($z(\varphi)$) in the rotating azimuthal plane (Fig. 1.b) using the associated polar angles ($\{\varphi_i\}_{i=\overline{0,N_i}}$). The projected planar polar path on the plane Oxy (Fig. 1.c) can be expressed as a quintic Hermite-type polynomial [2,6,8,10,32] defined by

$$r(\theta) = \sum_{k=0}^{q} u_k^i (\theta - \theta_i)^k \tag{2}$$

where q is the polynomial order (order 5 has been considered here), $u_0^i = r_i$ is the distance length between origin O and the via-point P_i, $u_1^i = \dot{r}_i$, $u_2^i = \ddot{r}_i$, $u_3^i = \frac{1}{2h_{ui}}[\ddot{r}_{i+1} - 3\ddot{r}_i] + \frac{2}{h_{ui}^2}[5r_i - 3\dot{r}_i - 2\dot{r}_{i+1}]$, $u_4^i = \frac{1}{2h_{ui}^2}[-2\ddot{r}_{i+1} + 3\ddot{r}_i] + \frac{1}{h_{ui}^3}[-15r_i + 8\dot{r}_i + 7\dot{r}_{i+1}]$, $u_5^i = \frac{1}{2h_{ui}^3}[\ddot{r}_{i+1} - \ddot{r}_i] + \frac{3}{h_{ui}^4}[2r_i - \dot{r}_i - \dot{r}_{i+1}]$, $u_0^{i+1} = r_{i+1}$ is the distance from the origin O to the via-point P_i, $u_1^{i+1} = \dot{r}_{i+1}$, $h_{ui} = \theta_{i+1} - \theta_i$, and $r_i = \frac{1}{h_{ui}}[r_{i+1} - r_i]$.

Trajectory height of the trajectory of motion is computed in the rotating plane (Fig. 1.b). The computation is performed using piecewise a piecewise polar interpolant expressed as a quintic Hermite polynomial [2,6,10,32] defined by

$$z(\varphi) = \sum_{k=0}^{q} s_k^i (\varphi - \varphi_i)^k \tag{3}$$

where $s_5^i = \frac{1}{2h_{si}^3}[\ddot{z}_{i+1} - \ddot{z}_i] + \frac{3}{h_{si}^4}[2z_i - \dot{z}_i - \dot{z}_{i+1}]$, $s_4^i = \frac{1}{2h_{si}^2}[-2\ddot{z}_{i+1} + 3\ddot{z}_i] + \frac{1}{h_{si}^3}[-15z_i + 8\dot{z}_i + 7\dot{z}_{i+1}]$, $s_3^i = \frac{1}{2h_{si}}[\ddot{r}_{i+1} - 3\ddot{z}_i] + \frac{2}{h_{si}^2}[5z_i - 3\dot{z}_i - 2\dot{z}_{i+1}]$, $s_2^i = \ddot{z}_i$, $s_1^i = \dot{z}_i$, $s_0^i = z_i$, $h_{si} = \varphi_{i+1} - \varphi_i$, and $z_i = \frac{1}{h_{ui}}[z_{i+1} - z_i]$.

2.2. Parametric model

One can parameterize the geometric path of the end using the cylindrical coordinate

$$\mathbf{r} = r(\theta)\cos(\theta)\,\mathbf{i} + r(\theta)\sin(\theta)\,\mathbf{j} + z(\varphi)\,\mathbf{k} \tag{4}$$

or equivalent

$$\mathbf{r} = \left(\sum_{k=0}^{5} u_k^i (\theta - \theta_i)^k \cos(\theta)\right)\mathbf{i} + \left(\sum_{k=0}^{5} u_k^i (\theta - \theta_i)^k \sin(\theta)\right)\mathbf{j} + \sum_{k=0}^{5} s_k^i (\varphi - \varphi_i)^k\,\mathbf{k} \tag{5}$$

One can now calculate the velocity vector [10] as $\mathbf{v}=\dot{\mathbf{r}}$, that is

$$\begin{aligned}
\mathbf{v} &= \left(-r\dot{\theta}\sin(\theta) + \dot{r}\cos(\theta)\right)\mathbf{i} + \left(r\dot{\theta}\cos(\theta) + \dot{r}\sin(\theta)\right)\mathbf{j} + \dot{z}(\varphi)\,\mathbf{k} \\
&= \left[\dot{\theta}\sum_{k=0}^{5} u_k^i k (\theta - \theta_i)^{k-1}\cos(\theta) \;\; -\dot{\theta}\sum_{k=0}^{5} u_k^i (\theta - \theta_i)^k \sin(\theta)\right]\mathbf{i} \\
&+ \left[\dot{\theta}\sum_{k=0}^{5} u_k^i k (\theta - \theta_i)^{k-1}\sin(\theta) \;\; +\dot{\theta}\sum_{k=0}^{5} u_k^i (\theta - \theta_i)^k \cos(\theta)\right]\mathbf{j} \\
&+ \left[\dot{\varphi}\sum_{k=0}^{5} s_k^i k (\varphi - \varphi_i)^{k-1}\right]\mathbf{k}
\end{aligned} \tag{6}$$

where $\dot{r}(\theta)$ and $\dot{z}(\varphi)$ are calculated from Eq. (2) and respectively Eq. (4) with $\dot{r}(\theta) = \dot{\theta}\sum_{k=0}^{5} u_k^i k\,(\theta-\theta_i)^{k-1}$ and $\dot{z}(\varphi) = \dot{\varphi}\sum_{k=0}^{5} s_k^i k\,(\varphi-\varphi_i)^{k-1}$.

The acceleration vector [10] can be calculated as

$$\begin{aligned}
\mathbf{a} = &\left[\left(\ddot{\theta}\sum_{k=0}^{5} p_k^i k\,(\theta-\theta_i)^{k-1} \;+\dot{\theta}^2\sum_{k=0}^{5} p_k^i\,(k-1)\,k\,(\theta-\theta_i)^{k-2} \;-\dot{\theta}^2\sum_{k=0}^{5} p_k^i\,(\theta-\theta_i)^{k}\right)\cos(\theta)\right]\mathbf{i}\\
&-\left[\left(2\dot{\theta}^2\sum_{k=0}^{5} p_k^i k\,(\theta-\theta_i)^{k-1} \;+\ddot{\theta}\sum_{k=0}^{5} p_k^i\,(\theta-\theta_i)^{k}\right)\sin(\theta)\right]\mathbf{i}\\
&+\left[\left(\ddot{\theta}\sum_{k=0}^{5} p_k^i k\,(\theta-\theta_i)^{k-1} \;+\dot{\theta}^2\sum_{k=0}^{5} p_k^i\,(k-1)\,k\,(\theta-\theta_i)^{k-2} \;-\dot{\theta}^2\sum_{k=0}^{5} p_k^i k\,(\theta-\theta_i)^{k}\right)\sin(\theta)\right]\mathbf{j}\\
&+\left[\left(2\dot{\theta}^2\sum_{k=0}^{5} p_k^i k\,(\theta-\theta_i)^{k-1} \;+\ddot{\theta}\sum_{k=0}^{5} p_k^i\,(\theta-\theta_i)^{k}\right)\cos(\theta)\right]\mathbf{j}\\
&+\left[\ddot{\varphi}\sum_{k=0}^{5} s_k^i k\,(\varphi-\varphi_i)^{k-1} \;+\dot{\varphi}^2\sum_{k=0}^{5} s_k^i k\,(k-1)\,(\varphi-\varphi_i)^{k-2}\right]\mathbf{k}
\end{aligned} \tag{7}$$

where the second derivatives $\ddot{r}(\theta)$ and $\ddot{z}(\varphi)$ are calculated using

$$\begin{aligned}
\ddot{r}(\theta) &= \ddot{\theta}\sum_{k=0}^{5} u_k^i k\,(\theta-\theta_i)^{k-1} + \dot{\theta}^2\sum_{k=0}^{5} u_k^i(k-1)k\,(\theta-\theta_i)^{k-2}\\
\ddot{z}(\varphi) &= \ddot{\varphi}\sum_{k=0}^{5} s_k^i k\,(\varphi-\varphi_i)^{k-1} + \dot{\varphi}^2\sum_{k=0}^{5} s_k^i(k-1)k\,(\varphi-\varphi_i)^{k-2}.
\end{aligned} \tag{8}$$

2.3. Forward kinematic equations and inverse kinematics in the rotating radial plane

To describe the forward kinematics in the rotating azimuthal plane, the geometrical parameters of the robotic arm modeled using n rigid rods (links) are needed. Each rod i has the length d_i and is linked to the rod $i+1$ with a joint. The position of each link (center of the mass or the end of the link) can be calculated using the lengths d_i of each link and the relative angles Φ_i between the links. The absolute angle Φ showing the end-effector direction is the summation of all the relative angles Φ_i between the links, as shown in Fig. 2

To describe the orientation of the rotating azimuthal plane a moving (rotating about the Oz axis) reference frame $Ox_ry_rz_r$ described by the unit vectors $[\mathbf{i}_r, \mathbf{j}_r, \mathbf{k}_r]$ is chosen. The unit vectors $[\mathbf{i}_r, \mathbf{j}_r, \mathbf{k}_r]$ of the moving reference frame can be computed with the unit vectors $[\mathbf{i}, \mathbf{j}, \mathbf{k}]$ of the fixed frame $Oxyz$ by the use the Euler angles

$$\begin{bmatrix} \mathbf{i}_r \\ \mathbf{j}_r \\ \mathbf{k}_r \end{bmatrix} = \begin{bmatrix} \cos(\theta) & -\sin(\theta) & 0 \\ \sin(\theta) & \cos(\theta) & 0 \\ 0 & 0 & 1 \end{bmatrix} \begin{bmatrix} \mathbf{i} \\ \mathbf{j} \\ \mathbf{k} \end{bmatrix}$$

For the robotic arm with i links, the kinematic equations written in the rotating azimuthal plane described by the unit vectors $[\mathbf{i}_r, \mathbf{j}_r, \mathbf{k}_r]$ can be expressed as

$$\begin{aligned}
r(\theta) &= \sum_{j=1}^{i} d_i \cos\left(\sum_{k=1}^{j} \Phi_i\right),\\
z(\varphi) &= \sum_{j=1}^{i} d_i \sin\left(\sum_{k=1}^{j} \Phi_i\right),\\
\Phi &= \sum_{k=1}^{i} \Phi_i
\end{aligned} \tag{9}$$

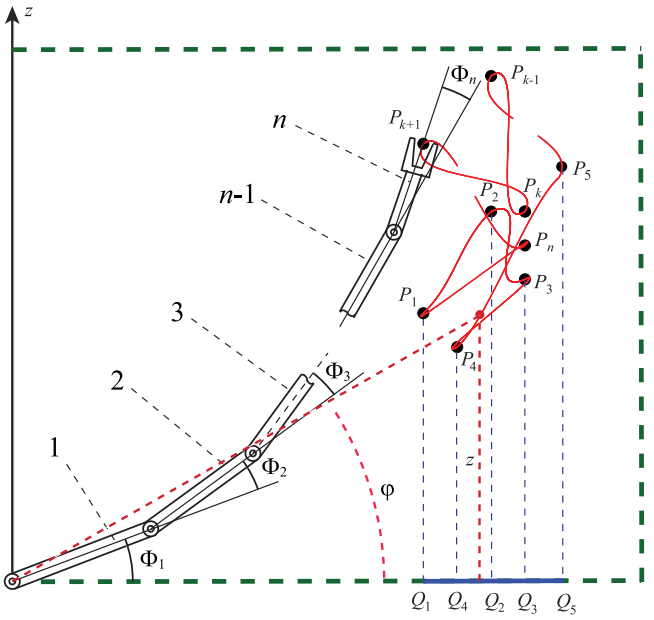

Fig. 2. Robotic arm modeled using n rigid links in the rotating azimuthal plane. The trajectory of the end effector in the rotating azimuthal plane is also shown.

In following the planar geometric path from one position to another the velocity of the end effector in the rotating azimuthal plane can be written as

$$\begin{aligned}
\dot{r}\,(\theta) &= -\sum_{j=1}^{i} d_i \left(\sum_{k-1}^{j} \dot{\Phi}_i\right) \sin\left(\sum_{k=1}^{j} \Phi_i\right),\\
\dot{z}\,(\varphi) &= \sum_{j=1}^{i} d_i \left(\sum_{k-1}^{j} \dot{\Phi}_i\right) \cos\left(\sum_{k=1}^{j} \Phi_i\right),\\
\dot{\Phi} &= \sum_{k=1}^{i} \dot{\Phi}_i
\end{aligned} \tag{10}$$

For a robotic manipulator with $i = 3$ links of lengths d_1, d_2 and d_3 the velocity and the acceleration between the end effector and joints calculated in the rotating azimuthal plane can be written as

$$\begin{bmatrix} \dot{r}\,(\theta) \\ \dot{z}\,(\varphi) \\ \dot{\Phi} \end{bmatrix} = \mathbf{J}\,(\Phi) \begin{bmatrix} \dot{\Phi}_1 \\ \dot{\Phi}_2 \\ \dot{\Phi}_3 \end{bmatrix} \tag{11}$$

$$\begin{bmatrix} \ddot{r}\,(\theta) \\ \ddot{z}\,(\varphi) \\ \ddot{\Phi} \end{bmatrix} = \mathbf{J}\,(\Phi) \begin{bmatrix} \ddot{\Phi}_1 \\ \ddot{\Phi}_2 \\ \ddot{\Phi}_3 \end{bmatrix} + \dot{\mathbf{J}}\,(\Phi) \begin{bmatrix} \dot{\Phi}_1 \\ \dot{\Phi}_2 \\ \dot{\Phi}_3 \end{bmatrix} \tag{12}$$

The Jacobian matrix of the robotic manipulator $\mathbf{J}\,(\Phi)$ in Eq. (11) is

$$\mathbf{J}\,(\Phi) = \begin{bmatrix} -S_1 & -S_2 & -S_3 \\ C_1 & C_2 & C_3 \\ 1 & 1 & 1 \end{bmatrix} \tag{13}$$

where S_m and C_m are calculated with

$$S_m = \sum_{j=m}^{n=3} d_j \sin\left(\sum_{k=1}^{j} \Phi_i\right)$$
$$C_m = \sum_{j=m}^{n=3} d_j \cos\left(\sum_{k=1}^{j} \Phi_i\right) \tag{14}$$

for any $m = 1, 2, 3$.

Inverse kinematics is the method used to compute the coordinates of the joints of the robotic arm for a given set of end effector coordinates. The calculation of the joint angles $\mathbf{\Phi_i}$, i=1,2,3, for a robotic manipulator with 3 links in the rotating azimuthal plane described by the unit vectors [i_1, j_1, k_1] frame is given by

$$\Phi_1 = \tan^{-1}\left(\frac{N_\Phi}{D_\Phi}\right) - \cos^{-1}\left(\frac{D_\Phi^2 + N_\Phi^2 + d_1^2 - d_2^2}{2d_1\sqrt{D_\Phi^2 + N_\Phi^2}}\right)$$
$$\Phi_2 = \pi - \left(\frac{d_1^2 + d_2^2 - (D_\Phi)^2 - (N_\Phi)^2}{2d_1 d_2}\right)$$
$$\Phi_3 = \Phi - \Phi_1 - \Phi_2 \tag{15}$$

where N_Φ and D_Φ are calculated by

$$N_\Phi = z(\varphi) - d_3 \sin(\Phi) = \sum_{k=0}^{q} s_k^i (\varphi - \varphi_i)^k - d_3 \sin(\Phi)$$
$$D_\Phi = r(\theta) - d_3 \cos(\Phi) = \sum_{k=0}^{q} u_k^i (\theta - \theta_i)^k - d_3 \cos(\Phi)$$

From Eqs. (11) and (6) the velocity of the joints for a robotic manipulator with 3 links following the desired trajectory in Eq. (1) can be calculated as

$$\begin{bmatrix} \dot{\Phi}_1 \\ \dot{\Phi}_2 \\ \dot{\Phi}_3 \end{bmatrix} = [\mathbf{J}(\Phi)]^{-1} \begin{bmatrix} \dot{\theta} \sum_{k=0}^{q} u_k^i k (\theta - \theta_i)^{k-1} \\ \dot{\varphi} \sum_{k=0}^{q} s_k^i k (\varphi - \varphi_i)^{k-1} \\ \dot{\Phi} \end{bmatrix}. \tag{16}$$

2.4. Inverse dynamics

Analogue to kinematics, one can find the solution to dynamics analysis problems by forward (or direct) dynamics or by inverse dynamics. While forward dynamics determine the motion of robot manipulator using the specified external forces and torques the inverse dynamics assess the joint torques considering the acceleration, velocity and position of the end-effector.

The inverse dynamics of the robotic manipulator [21,26,27] can be written using

$$\tau_i = \frac{d}{dt}\left(\frac{\partial \mathcal{L}}{\partial \dot{\Phi}_i}\right) - \frac{\partial \mathcal{L}}{\partial \Phi_i} \tag{17}$$

where $\mathcal{L}(\Phi, \dot{\Phi}) = \mathcal{T}(\Phi, \dot{\Phi}) - \mathcal{U}(\Phi)$ represents the Lagrangian quantified as the difference between total kinetic $\mathcal{T}$ and potential $\mathcal{U}$ energy of the manipulator.

The total kinetic and potential energy of the robotic manipulator [26] with n links is calculated with

$$\begin{aligned}\mathcal{T} &= \sum_{i=1}^{n} \mathcal{T}_i \\ &= \sum_{i=1}^{n} \left(\frac{1}{2} m_i \mathbf{v}_{c_i}^T \mathbf{v}_{c_i} + \frac{1}{2} m_i \omega_i^T \mathbf{I}_i \omega_i \right) \\ &= \frac{1}{2} \dot{\Phi}^{\mathbf{T}} \mathbf{H} \dot{\Phi} \\ \mathcal{U} &= \sum_{i=1}^{n} -m_i \mathbf{g}^T \mathbf{r}_{0c_i} \end{aligned} \tag{18}$$

where $\mathbf{r}_{0c_i}$ represents the position vector of the centroid of link i, $\mathbf{v}_{c_i} = \mathbf{J}_i^L \dot{\Phi}$ is the velocity vector, $\omega_i = \mathbf{J}_i^A \dot{\Phi}$ is the angular velocity vector, $\mathbf{J}_i^L$ is the centroidal linear velocity Jacobian matrix, $\mathbf{J}_i^A$ is the centroidal angular velocity Jacobian matrix, $\mathbf{I}_i$ is the inertia matrix of the ith link, $\mathbf{H} = \sum_{i=1}^{n} \left(m_i \mathbf{J}_i^{L^T} \mathbf{J}_i^L + \mathbf{J}_i^{A^T} \mathbf{I}_i \mathbf{J}_i^A \right)$ is the inertia matrix.

Replacing Eq. (18), i.e., the values of the kinetic and potential energy, and the components of the multibody inertia matrix $\mathbf{H} = \{H_{ij}\}$, in Eq. (17) one can obtain

$$\tau_i = \sum_{i=1}^{n} H_{ij} \ddot{\Phi}_j + \sum_{i=1}^{n} \frac{\partial H_{ij}}{\partial \Phi_k} \left(\dot{\Phi}_j \right)^2 + \frac{1}{2} \sum_{j=1}^{n} \sum_{k=1}^{n} \frac{\partial H_{jk}}{\partial \Phi_i} \dot{\Phi}_j \dot{\Phi}_k + G_i \tag{19}$$

or equivalent in a matrix form [27]

$$\tau_i = M \begin{bmatrix} \ddot{\Phi}_1 \\ \vdots \\ \ddot{\Phi}_n \end{bmatrix} + \hat{C} \begin{bmatrix} \dot{\Phi}_1 \\ \vdots \\ \dot{\Phi}_n \end{bmatrix} + \tilde{C} \begin{bmatrix} \dot{\Phi}_1 \dot{\Phi}_2 \\ \vdots \\ \dot{\Phi}_{n-1} \dot{\Phi}_n \end{bmatrix} + \begin{bmatrix} G_1 \\ \vdots \\ G_n \end{bmatrix} \tag{20}$$

where M is the matrix of inertia, $\hat{C}$ and $\tilde{C}$ are the centripetal and the Coriolis force matrices, and $G_i = \dfrac{\partial U}{\partial \Phi_i}$ is the gravity vector. The total kinetic energy and potential energy for a robotic manipulator with 3 links of lengths d_1, d_2 and d_3 can be calculated as

$$\begin{aligned}\mathcal{T} &= \sum_{i=1}^{3} \left(\frac{1}{2} m_i v_i^2 + \frac{1}{2} m_i \sum_{k=1}^{i} \dot{\Phi}_k \right) \\ \mathcal{U} &= -\sum_{i=1}^{3} m_i g \sum_{k=1}^{i} \frac{1}{2} d_i \sin \left(\sum_{k=1}^{i} \Phi_i \right) \end{aligned} \tag{21}$$

where Φ_i was calculated in Eq. (15) and $\dot{\Phi}_k$ was calculated in Eq. (16), and the torque τ_i can be calculated similar to [1].

3. Optimization techniques

Since the inverse kinematics of the robotic arm is undetermined, an infinite number of solutions exist depending upon the orientation of the end effector described by the angle Φ which can be expressed as piecewise polynomial with a zero angular velocity at the start and at the end of the task.

3.1. Damped least square (DLS) method

The DLS method generally used to solve non-linear least squares problems was considered in inverse kinematics to minimize large values of joint velocities by diverging from the desired path [13].

The use of damping factor is relevant in assessing the viability and accuracy of joint velocities in order to avoid large deviations of the trajectory by considering the function objective of the optimization problem formulated as

$$\mathcal{R} = \| \mathbf{v} - \mathbf{J}_i^A \dot{\Phi} \| + \lambda \| \dot{\Phi} \|^2 \tag{22}$$

where $\|.\|$ is the associated euclidian norm and the damping factor λ is determined as a function of the smallest singular value of $\mathbf{J}_i^A$ used to optimize $\mathcal{R}$. A value of 0.02 was considered along the study for the damping factor λ.

3.2. End-effector position error minimization

Considering joint angle displacements between successive locations the end-effector positioning error could be minimize [2] by considering the function objective of the optimization problem defined as

$$\mathcal{R} = w_1\mathcal{E}_e + w_2\mathcal{D}_j + w_3\mathcal{V}_e + w_4\mathcal{V}_j \tag{23}$$

where w_i are weighting factors to satisfy $\sum_{i=1}^{n} w_i = 1$. The variable $\mathcal{E}_e$ is calculated using $\mathcal{E}_e = \sum_{i=1}^{n} \sqrt{\left(r(\theta) - r_g(\theta)\right)^2 + \left(z(\phi) - z_g(\phi)\right)^2}$, where $r_g(\theta)$ and $z_g(\phi)$ are the generated end effector positions in the rotating azimuthal plane. The variable $\mathcal{D}_j$ calculated as $\mathcal{D}_j = \sum_{i=1}^{n-1} \left(\Phi_j^{i+1} - \Phi_j^i\right)^2$ is used to minimize joint displacement along the trajectory, j is the related joint link, i and $i+1$ are two successive positions of the link j. The variable $\mathcal{V}_e$ is the velocity of the end effector, and the variable $\mathcal{V}_j = \sum_{i=1}^{n-1} \left|\Phi_j^{i+1} - \Phi_j^i\right|$ represents the angular joint displacement.

3.3. Minimum consumed power

To advance the end-effector along the appropriate trajectory with minimum consumed power [27] the objective of optimization problem could be presented as

$$\mathcal{R} = \sum \left|\dot{\Phi}_i^2 \tau_i^2\right| \tag{24}$$

where τ_i and $\dot{\Phi}_i$ are the applied torque and the angular velocity of the ith joint.

3.4. Optimal traveling time with minimization of the mechanical energy

Optimal traveling time [26] of a robotic manipulator is obtained by minimizing the associated time intervals t_1, t_2, …, t_n corresponding to the motion between the via-points P_m, $m = 1, \ldots, n$ of the trajectory.

The total time computed along the trajectory [26] that maximize the working speed of the robotic manipulator can by presented as an optimization problem defined for the time intervals t_i as

$$\mathcal{R} = \delta_1 \sum_{i=1}^{n-1} t_i + \delta_2 \sum_{i=1}^{n-1} \left(\tau_i^T \dot{\Phi}_i\right)^2 t_i \tag{25}$$

subject to velocity, acceleration and jerk constraints [26]. The variables δ_1 and δ_2 in Eq. (25) are the weighting factors usually taken between 0 and 1, the variables τ_i are the applied torques, and the variables $\dot{\Phi}_i$ represent the angular velocities of the rotational joints.

4. Results

The smooth end-effector trajectory and joints trajectory generation, as well as the optimization of joints trajectory, are implemented in Matlab [20] using a numerical approach. For the numerical study the robotic manipulator is

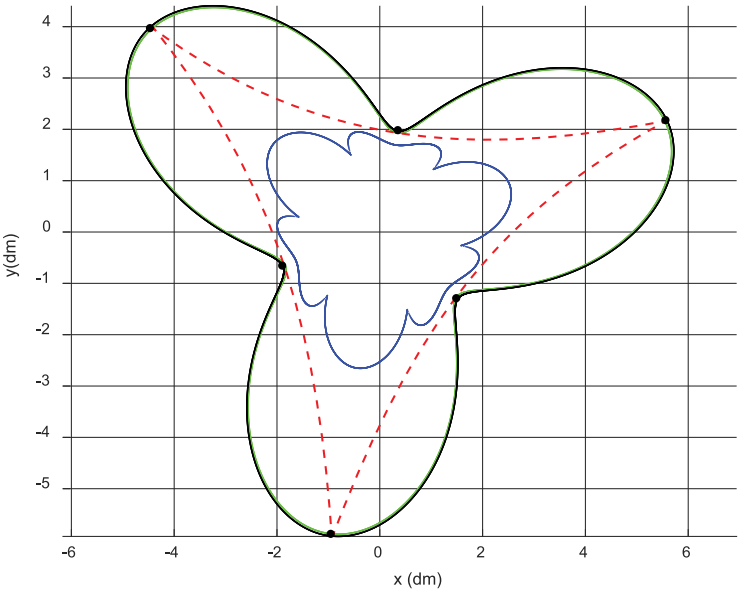

Fig. 3. Trajectory of the end effector (black) and trajectory of the 2nd joint (blue). (For interpretation of the references to color in this figure legend, the reader is referred to the web version of this article.)

Table 1
Via-points i to be reached by the end-effector, for radial distance r_i (decimeters) polar angles θ_i (degrees) and heights z_i ((decimeters)).

Var					Value		
i	1	2	3	4	5	6	7
θ_i	80	140	200	260	320	380	440
r_i	2	6	2	6	6	6	2
z_i	2	4	2	4	2	4	2

composed of 4 links, link 1 is as vertical rotating link of height $d_1 = 0.005$ m and radius $r_1 = 0.025$ m, link 2 of length $d_2 = 0.2$ m and radius $r_2 = 0.0035$ m, link 3 of length $d_3 = 0.3$ m and radius $r_3 = 0.0035$ m, and the end-effector link 4 of length $d_4 = 0.02$ m and radius $r_4 = 0.0025$ m, all of them made from steel with a density of 7900 kg/m^3. The moment of inertia about the central axis for link 2 and link 3 are $I_{central-axis_2} = 3.72$ kg m^2, and link 3 is having $I_{central-axis_3} = 5.58$ kg m^2. Using the polar angles θ_i, the radial distances r_i and the heights z associated to the azimuthal angles, a smooth end-effector trajectory of the robotic arm is generated along the considered via-points denoted by i.

The trajectory is a merger of the coordinates of the radial distance in the plane Oxy derived by Hermite piecewise polar interpolation in Eq. (1), and the coordinate of the height calculated in the rotating azimuthal plane by the Hermite piecewise polar interpolation shown Eq. (4). To illustrate end-effector trajectory and joints trajectory generation, as well as the optimization of joints trajectory, three numerical examples are considered.

Example 1

In this case all the via points could be potentially located on a tricuspid path (red dotted line) and the end effector should connect the via points by a smooth trajectory. For simplicity just 6 points have been considered, with three of them being the vertices of the imaginary path. The radial distances r_i (in decimeters) associated to the polar angles θ_i (in degrees) and the end effector heights z_i (in decimeters) are presented in Table 1.

The algorithm connected the via points i (Table 1) by a 3D end-effector path (black curve) as shown in Fig. 3. The 2nd joint trajectory (blue curve) is also shown in Fig. 3. Studying the resulting path of end-effector (black curve), one can see that the trajectory does not followed the imaginary tricuspid path when crossing the singularities at the

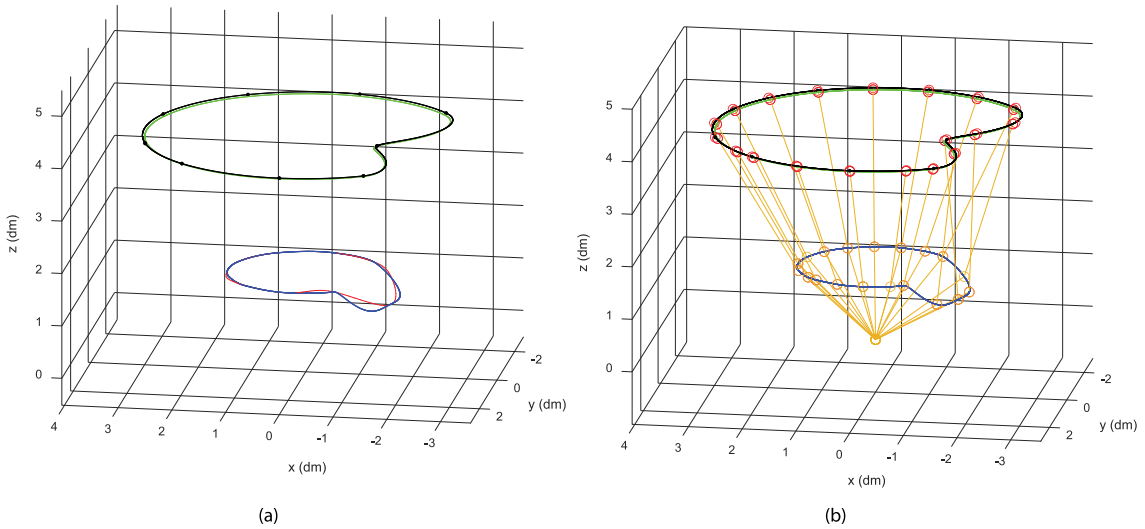

Fig. 4. (a) trajectory of the end effector (black), joints (blue and green) and, optimized trajectory of the joint (red), (b) trajectories of end effector and joints, and manipulator arm configuration. (For interpretation of the references to color in this figure legend, the reader is referred to the web version of this article.)

Table 2
Via-points i to be reached by the end-effector, for radial distance r_i (decimeters), polar angles θ_i (degrees), and heights z_i (decimeters).

Var	Value									
i	1	2	3	4	5	6	7	8	9	10
θ_i	20	50	90	120	160	220	260	300	340	360+20
r_i	3	3	3	3	1.5	3	3	3	3	3
z_i	4	4	4	4	4	4	4	4	4	4

vertices (cusp singular points where the motion of the end-effector is very slow) and instead created a semicircular path (as expected) in order to produce smoothness.

Example 2

In this case all the via point are planar (on a plane parallel with the Oxy plane) and all but one are located on a circular trajectory as shown in Fig. 4. The radial distances r_i, associated polar angles θ_i and end effector heights z_i – linked to the related via-points the robotic manipulator should follow – are presented in Table 2.

The smooth 3D end-effector path (black curve), joints' trajectories (green and blue curves) and optimized joint trajectory (red curve) - for the robotic manipulator following the via-points positions in Table 2 - are shown in Fig. 4.a. Fig. 4.b presenting the end effector and joints' trajectories also presents the manipulator arm configuration (links) along the motion.

Example 3

This is a general case showing random via points located in the 3D space (Fig. 5.a and Fig. 5.b). In this case the radial distances r_i which are correlated with the polar angles θ_i and the end effector heights z_i are shown in Table 3.

For this general case the base of the manipulator is located at the origin of the reference frame. As shown in Fig. 5.a the algorithm connected the via points i (Table 3) by a 3D end-effector path (black curve). Fig. 5.a also presents the joints' trajectories (blue and green curve) and optimized 2nd joint trajectory (red curve). Fig. 5.b presenting the end effector and joints' trajectories also presents the manipulator arm configuration (links) along the motion, while Fig. 5.c presents the relative angles (of the links) measured in the rotating azimuthal plane along the azimuthal angle.

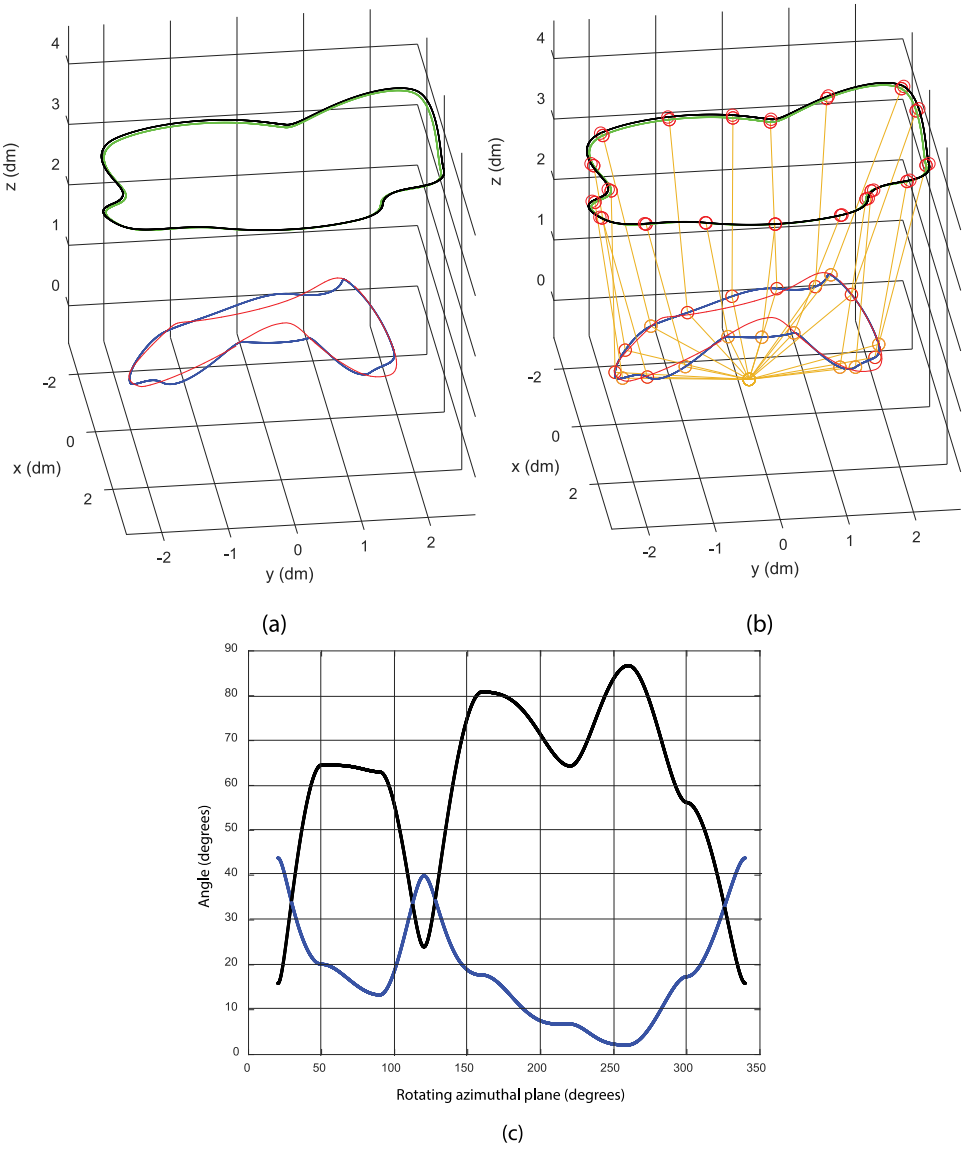

Fig. 5. (a) trajectory of the end effector (black), joints (blue and green) and optimized trajectory of the joint (red), (b) trajectories and manipulator arm configuration, and (c) Relative angles (of the links 2 and 3) along the robotic arm trajectory in the rotating azimuthal plane. (For interpretation of the references to color in this figure legend, the reader is referred to the web version of this article.)

Table 3
Via-points i to be reached by the end-effector, for radial distance r_i (decimeters), polar angles θ_i (degrees), and heights z_i (decimeters).

Var	Value									
i	1	2	3	4	5	6	7	8	9	10
θ_i	20	50	90	120	160	220	260	300	340	360+20
r_i	3	2.2	2.7	2.9	1.5	3	2.1	2.8	3	3
z_i	4	3.7	3.4	4	3.6	3.1	3.1	3.5	4	4

The direct connection (distances) between the origin O of the associated Cartesian reference frame and some random points along the end effector trajectory are shown in Fig. 6.a. For all the connected distances (some presented in Fig. 6.a) the angle against the projected horizontal directions is shown in Fig. 6.b.

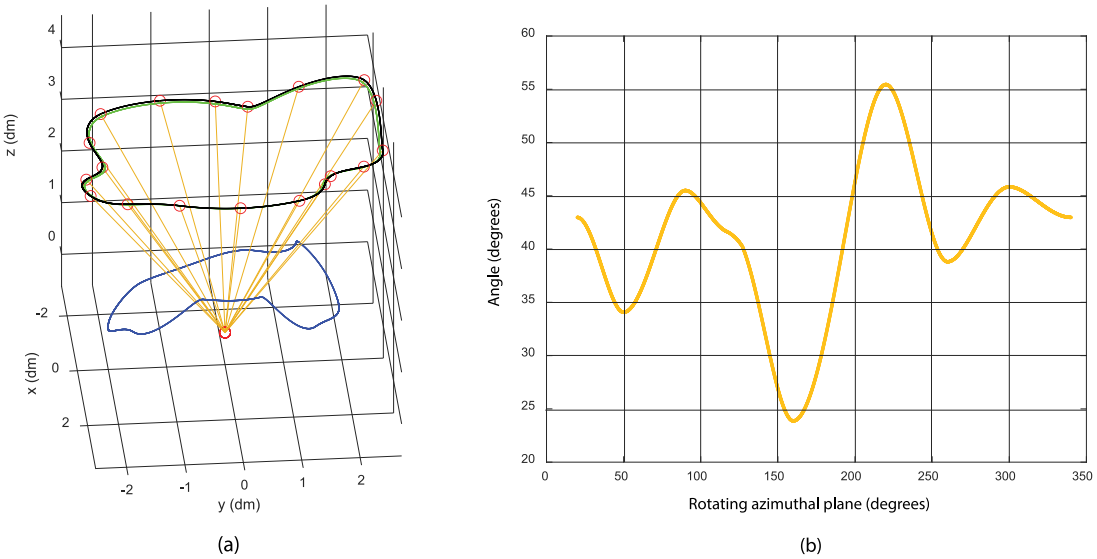

Fig. 6. (a) Direction rays towards the end-effector trajectory (from the origin O), and (b) Angle of the end-effector trajectory relative to the origin O in the rotating azimuthal plane.

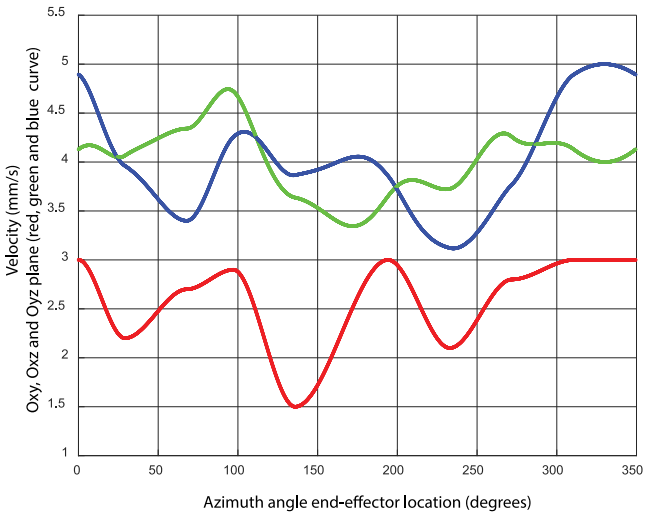

Fig. 7. Velocity of the end effector along the obtained trajectory. (For interpretation of the references to color in this figure legend, the reader is referred to the web version of this article.)

The velocity projection on the Oxy, Oxz, and Oyz planes denoted by v_{xy} (red curve), v_{xz} (blue curve), and v_{yz} (green curve) is shown in Fig. 7. The simulation in Fig. 7 have shown a continuous velocity profile for each velocity projection, that is, a strong evidence of a smooth trajectory.

5. Conclusion

In this study, the 3D path planning along with the inverse kinematics and dynamics of a redundant robotic manipulator is examined. The developed approach consider manipulator geometry and a spherical coordinate system for the initial smooth trajectory generation along the 3D via points by merging Hermite-type polar piecewise interpolation curves computed in the fixed radial and rotating azimuthal planes. While previous approaches addressed the modeling and simulation by combining (a) the zenithal gnomic trajectory (located on a projective plane) and

the related azimuthal trajectory (generated by polar piecewise interpolation on the azimuthal angles)[9], or (b) the radial trajectory (generated by polar piecewise interpolation) and the related height (calculated in a normal plane unfolded along the radial trajectory of the motion)[6], the actual approach generates a more efficient computational approach by combining the radial distance (obtained by using the azimuthal angles) and the corresponding height (obtained by using the corresponding polar angles computed in the rotating azimuthal plane).

Trajectory smoothness achieved by quintic Hermite piecewise interpolation unveiling continuous derivatives and generated by inverse kinematics or dynamics are accurate and suitable to a numerical implementation. Optimization solutions to minimize the joint velocities, the end-effector positioning error, the traveling time and mechanical energy, or the consumed power, are surveyed. Numerical examples are presented to assess the smooth trajectory planning of the end effector, computation of the joints trajectory and the optimal trajectory with end-effector position error minimization and illustrate the proposed approach. The presented examples convey that the trajectory planning, and inverse kinematics and dynamics used in the proposed approach could be successfully applied on the redundant robotic manipulator, consequently confirming the efficacity of the approach presented in this study.

Acknowledgments

The author would like to thank the three referees for the comments and suggestion that led to improvements in the quality of this paper.

References

[1] A.A. Ata, M.A. Ghazy, M.A. Gadou, Dynamics of a general multi-axis robot with analytical optimal torque analysis, J. Autom. Control Eng. 1 (2) (2013) 144–148.
[2] A.A. Ata, R.T. Myo, Optimal point-to-point trajectory tracking of redundant manipulators using generalized pattern search, Int. J. Adv. Robot. Syst. 2 (3) (2005) 239–244.
[3] T. Balkan, M.K. Özgören, M.S. Arıkan, H.M. Baykurt, A kinematic structure-based classification and compact kinematic equations for six-dof industrial robotic manipulators, Mech. Mach. Theory 36 (7) (2001) 817–832.
[4] M. Boryga, A. Grabos, Planning of manipulator motion trajectory with higher-degree polynomials use, Mech. Mach. Theory 44 (2009) 1400–1419.
[5] C.A.A. Calderon, E.M.R.P. Alfaro, J.Q. Gan, H. Hu, 'Trajectory generation and tracking of a 5-DOF robotic arm', CONTROL, 2004.
[6] M. Dupac, A virtual prototype of a constrained extensible crank mechanism: Dynamic simulation and design, Proc. Inst. Mech. Eng. K 227 (3) (2013) 201–210.
[7] M. Dupac, A path planning approach of 3D manipulators using zenithal gnomic projection and polar piecewise interpolation, Math. Methods Appl. Sci. 41 (17) (2018) 7202–7213.
[8] M. Dupac, Smooth trajectory generation for rotating extensible manipulators, Math. Methods Appl. Sci. 41 (6) (2018) 2281–2286.
[9] M. Dupac, A combined polar and Cartesian piecewise trajectory generation and analysis of a robotic arm, Comput. Math. Methods 1 (5) (2019) 1–10.
[10] M. Dupac, 3D curve generation using spherical polar piecewise interpolation in CAD and CAM, Appl. Mech. Mater. 896 (2020) 224–228.
[11] Y. Fang, J. Hu, J. Qi, W. Liu, W. Wang, Y. Peng, Planning trigonometric frequency central pattern generator trajectory for cyclic tasks of robot manipulators, Proc. Inst. Mech. Eng. C 233 (11) (2019) 4014–4031.
[12] A. Gasparetto, V. Zanotto, A new method for smooth trajectory planning of robot manipulators, Mech. Mach. Theory 42 (2007) 455–471.
[13] L. Gracia, J. Andres, J. Tornero, Trajectory tracking with a 6R serial industrial robot with ordinary and non-ordinary singularities, Int. J. Control Autom. Syst. 7 (1) (2009) 85–96.
[14] M. Gross, A. Staniforth, Cubic-spline interpolation on a non-uniform latitude–longitude grid: achieving cross- and circum-polar continuity, Atmos. Sci. Let. 11 (2010) 229–238.
[15] Y. Iwashita, Piecewise polynomial interpolation, OpenGamma Quant. Res. 15 (2014) 1–22, http://www.opengamma.com/research.
[16] A.H. Khan, S. Li, X. Luo, Obstacle avoidance and tracking control of redundant robotic manipulator: An RNN-based metaheuristic approach, IEEE Trans. Ind. Inform. 16 (7) (2019) 4670–4680.
[17] D. Kiritsis, High precision interpolation algorithm for 3D parametric curve generation, Comput. Aided Des. 26 (1) (1994) 850–856.
[18] J.L. Lavery, Univariate cubic L_p splines and shape-preserving, multiscale interpolation by univariate cubic L_1 splines, Comput. Aided Geom. Design 17 (2000) 319–336.
[19] J.L. Lavery, Shape-preserving, multiscale interpolation by univariate curvature-based cubic L1 splines in Cartesian and polar coordinates, Comput. Aided Geom. Design 19 (2002) 257–273.
[20] D.B. Marghitu, M. Dupac, Advanced Dynamics: Analytical and Numerical Calculations with Matlab, Springer, New York, 2012.
[21] P.K. Nithya, P.S. Lal Priya, E.B. Gifty, J. Venkateswaran, Optimal path planning and static obstacle avoidance for a dual arm manipulator used in on-orbit satelite servicing, IFAC Papers OnLine 53 (1) (2020) 189–194.
[22] V. Olunloyo, O. Ibidapo-obe, D. Olowookere, M. Ayomoh, —Inverse kinematics analysis of a five jointed revolute arm mechanism, J. Control Sci. Eng. 2 (2014) 7–15.

[23] C.M. Pappalardo, D. Guida, On the dynamics and control of underactuated nonholonomic mechanical systems and applications to mobile robots, Arch. Appl. Mech. 89 (4) (2019) 669–698.
[24] A. Piazzil, A. Visioli, A Global Optimization Approach to Trajectory Planning for Industrial Robots, IEEE, 1997.
[25] S. Pruess, Shape preserving c^2 cubic spline interpolation, IMA J. Numer. Anal. 13 (4) (1993) 493–507.
[26] S.F.P. Saramago, V. Steffen Jr., Optimization of the trajectory planning of robot manipulators taking into account the dynamics of the system, Mech. Mach. Theory 33 (7) (1998) 883–894.
[27] V.V.M.J. Satish Chembuly, H.K. Voruganti, Trajectory planning of redundant manipulators moving along constrained path and avoiding obstacles, Procedia Comput. Sci. 133 (2018) 627–634.
[28] H. Schaeben, A brief survey of spherical interpolation and approximation methods for texture analysis, Textures Microstruct. 25 (1996) 159–169.
[29] C.H. Sequin, K. Lee, J. Yen, Fair, G^2- and C^2-continuous circle splines for the interpolation of sparse data points, Comput. Aided Des. 37 (2005) 201–211.
[30] N. Tan, P. Yu, Robust model-free control for redundant robotic manipulators based on zeroing neural networks activated by nonlinear functions, Neurocomputing 438 (2021) 44–54.
[31] B. Tao, X. Zhao, S. Yan, H. Ding, Kinematic modeling and control of mobile robot for large-scale workpiece machining, Proc. Inst. Mech. Eng. B 236 (1–2) (2022) 29–38.
[32] L. Wang, C. Chen, A combined optimization method for solving the inverse kinematics problems of mechanical manipulators, IEEE Trans. Robot. Autom. 7 (4) (1991) 489–499.
[33] H. Wang, J. Huang, B. Zhao, L. Quan, Smooth point-to-point trajectory planning for industrial robots with kinematical constraints based on high-order polynomial curve, Mech. Mach. Theory 139 (2019) 284–293.
[34] D. Xu, C.A. Calderon, J. Gan, H. Hu, M. Tan, An analysis of the inverse kinematics for a 5-DOF manipulator, Int. J. Autom. Comput. 2 (2) (2005) 114–124.